The effect of MgO/TiO_2 on structural and crystallisation behaviour of near invert phosphate-based glasses

*Md Towhidul Islam[a], Nusrat Sharmin[b], Graham A. Rance[c], Jeremy J. Titman[d], Andrew J. Parsons[a], Kazi M. Zakir Hossain[a] and Ifty Ahmed[a]**

[a] Advanced Materials Research Group, Faculty of Engineering, University of Nottingham, Nottingham, NG7 2RD, UK

[b] Department of Chemical and Environmental Engineering, Faculty of Science and Engineering, University of Nottingham Ningbo China, Ningbo, China

[c] Nanoscale and Microscale Research Centre (nmRC), Cripps South, University Park, University of Nottingham, Nottingham, NG7 2RD, UK

[d] School of Chemistry, University of Nottingham, University Park, Nottingham, NG7 2RD, UK

email: Ifty.Ahmed@nottingham.ac.uk

Abstract

Varying formulations in the glass system of $40P_2O_5$-(24-x)MgO-(16+x)CaO-(20-y)Na_2O-yTiO_2 (where $0 \leq x \leq 22$ and y=0 or 1) were prepared via melt-quenching. The structure of the glasses was confirmed by X-ray diffraction (XRD), Fourier transform infrared (FTIR), micro Raman and solid-state nuclear magnetic resonance (NMR) spectroscopies. The thermal properties and the activation energy of crystallisation (E_c) were measured using thermal analysis and the Kissinger equation, respectively. The glass forming ability of the formulations investigated was seen to decrease with reducing MgO content down to 8 mol% and the glass stability region also decreased from 106 ^oC to 90 ^oC with decreasing MgO content. The activation energy of crystallisation (E_c) values also decreased from 248 (for 24 mol% MgO glass) to 229

kJ/mol (for the 8 mol% MgO content) with the replacement of MgO by CaO for glasses with no TiO_2. The formulations containing less than 8 mol% MgO without TiO_2 showed a strong tendency towards crystallisation. However, the addition of 1 mol% TiO_2 in place of Na_2O for these glasses with less than 8 mol% MgO content, inhibited their crystallisation tendency. Glasses containing 8 mol% MgO with 1 mol% TiO_2 revealed a 12 ^oC higher glass transition temperature, a 14 ^oC increase in glass stability against crystallisation and a 38 kJ/mol increase in E_c in comparison to their non TiO_2 containing counterpart. NMR spectroscopy revealed that all of the formulations contained almost equal percentages of Q^1 and Q^2 species. However, FTIR and Raman spectroscopies showed that the local structure of the glasses had been altered with addition of 1 mol% TiO_2, which acted as a network modifier, impeding crystallisation by increasing the cross-linking between phosphate chains and consequently leading to increased E_c as well as their glass forming ability.

Introduction

Phosphate-based glasses (PBGs) have attracted a lot of interest in the field of biomaterials and tissue engineering due to their controllable degradation profiles and chemical similarity with the inorganic component of natural bone [1-3]. PBGs with various modifying oxide such as CuO [4], ZnO [5], Ag_2O [6], Fe_2O_3 [7], TiO_2 [8], SrO [9], have been extensively investigated to adjust for biomedical and tissue engineering applications [10]. For example, the addition of CaO has been reported to improve the bioactivity of these glasses and to enhance haemostatic activity [11-14]. However, the glass structure could be disrupted due to the addition or replacement of modifying oxide and consequently, the glass forming ability could be decreased [15].

The structure of PBGs is composed of PO_4^{3-} tetrahedral units. The tetrahedra can be described in terms of Q^n terminology, where *n* represents the number of bridging oxygens (BOs) per PO_4^{3-} tetrahedron. In vitreous P_2O_5 each tetrahedral unit is connected with three others via bridging oxygen and the fourth oxygen of each tetrahedral unit is known as a non-bridging oxygen (NBOs) [16]. Phosphate tetrahedra with three bridging oxygens (BOs) are referred to as Q^3 species where the fraction O/P = 2.5. Addition of modifying oxides, such as CaO, disrupts the phosphate network and increases the O/P ratio. As the O/P ratio increases from 2.5 to 4 (2.5, 3, 3.5, 4) the phosphate structural group passes from Q^3 to Q^0 ($Q^3 \rightarrow Q^2 \rightarrow Q^1 \rightarrow Q^0$), where Q^0 represents isolated PO_4^{3-} units with four NBOs [17]. PBGs with smaller phosphate units can crystallise easily as compared to glasses with longer phosphate chains as the entangled chains of the long chain phosphate glasses increase the viscosity of melt and impede crystallisation [18].

However, vitreous P_2O_5 (i.e. with completely Q^3 structural unit) is chemically unstable, therefore modifying oxides have been added to make the PBG glass stable via the formation of P-O-M bonds (where M is a metal cation) [19]. The chemical durability and glass-forming ability of phosphate-based glasses has been reported to be significantly improved with the addition of TiO_2 [20,21]. Titanium can present in the glass as Ti^{4+} or Ti^{3+}, with the oxidation state of Ti in the glass dependent on the melting conditions (oxidizing or reducing) and the total amount of titanium present in the glass [22]. Ti^{4+} has also been reported to act as a glass former, whilst Ti^{3+} serves as a glass modifier [22]. In addition, titanium containing glasses have shown good cell viability, attachment and proliferation [8,23-26]. Abou Neel *et* al. studied the effect of TiO_2 on the cytocompatibility of P50Ca30$Na_2$0Ti0 glasses and reported that the addition of 5 to 15 mol% TiO_2 in place of Na_2O was effective in increasing cell viability [8]. It has also been

reported that TiO_2 in phosphate glasses could help to induce calcium phosphate surface nucleation and thus improve the bioactivity of glasses [27]. However, TiO_2 is also act as a nucleating agent and favors devitrification at local level for the silicate glasses [1-4]. Danewalia *et. al.* studied the incorporation of TiO2 in $45SiO_2$–25CaO– $10Na_2O$–$5P_2O_5$–$10MnO_2$–$5Fe_2O_3$ glass ceramic system on structural, magnetic and bioactive properties [1]. They found that the more ordered local structure of the glasses with increasing TiO_2 content from 1.25 to 5 wt% [1].

Crystallisation kinetics is an important topic for glass formation and glass-ceramic synthesis [28]. The glass forming ability of a composition can be assessed by its reluctance to undergo crystallisation [28]. The crystallisation process is usually described by the activation energy of crystallisation (E_c) and the Johnson-Mehl-Avrami (JMA) exponent (n). The E_c gives an indication of the temperature dependence of the crystallisation process, whereas n gives an idea on the crystal growth dimensionality [29]. The activation energy of crystallisation can be calculated using the Kissinger equation [30], amongst others. The JMA exponent can be calculated using the Augis and Bennett equation [31]. It is also worth noting that the crystallisation parameters can often be influenced by the size of glass particles [32,33]. The resistance of a glass against crystallisation can also be quantified in terms of the glass stability, which is the temperature difference between the glass transition (T_g) and the onset of crystallisation (T_x) [34].

The aim of this work was to investigate the effect of decreasing MgO content with CaO in the quaternary glass formulation of $40P_2O_5$-(24-x)MgO-(16+x)CaO-$20Na_2O$. However, reducing the MgO content to lower than 8mol% revealed that the glasses crystallised. As such, a further series of glasses were then evaluated incorporating 1 mol% TiO_2 (in the series $40P_2O_5$-(8-

x)MgO-(32+x)CaO-19Na_2O-TiO_2), to investigate if the crystallisation could be arrested. Thermal, physical (i.e. density) and structural analyses were conducted via simultaneous thermal analysis (SDT), the Archimedes method and X-ray diffraction (XRD), Fourier transform infrared (FTIR), Raman and nuclear magnetic resonance (NMR) spectroscopies, respectively.

Materials and Methodology

Glass Preparation

Varying formulations in the glass system $40P_2O_5$-(24-x)MgO-(16+x)CaO-(20-y)Na_2O-yTiO_2 (where $0 \leq x \leq 22$ and y=0 or 1) were prepared using sodium dihydrogen phosphate (NaH_2PO_4), calcium hydrogen phosphate ($CaHPO_4$), magnesium hydrogen phosphate trihydrate ($MgHPO_4.3H_2O$), phosphorous pentoxide (P_2O_5) and titanium dioxide (TiO_2) as starting materials (Sigma Aldrich, UK). The required amounts of precursors were weighed, mixed and transferred to a platinum rhodium alloy crucible (Birmingham Metal Company, U.K.) which was then placed into a furnace at 350 ^oC for 0.5 hours to remove H_2O. The mixture was then transferred to another furnace pre-heated to between 1150-1200 ^oC for 1.5-2 hours depending on the glass composition, as shown in Table 1. The resulting molten glass was poured onto a steel plate and left to cool to room temperature.

X-ray diffraction analysis

X-ray diffraction studies were conducted to confirm the amorphous nature of each glass formulation using a Bruker D8 Advanced diffractometer. The instrument was operated at room temperature and ambient atmosphere with Ni-filtered CuKα radiation (λ=0.15418 nm), generated at 40 kV and 35 mA. Scans were performed with a 5˚ glancing angle, a step size of 0.04° and a step time of 8 seconds over an angular range 2θ from 15° to 50°.

Density measurement

The density of the glasses was determined in accordance with the standard ASTMD-792 using the Archimedes method. The measurement was carried out at room temperature using industrial methylated spirit (IMS) as the immersion fluid. Bubble free glass rods (9×20 mm) were used for the experiment, which was repeated three times for each glass formulation. The density of glasses was calculated using equation 1:

$$\rho = \frac{\mathrm{A}}{\mathrm{A-B}} \times \rho_o \text{.....(1)}$$

Where A and B are the weight of the glass rods in air and in IMS respectively, and ρ_o is the density of IMS at the given temperature.

The compactness of a glass structure can be measured by the oxygen density of that glass [35-37].The oxygen density considers the effect of oxygen and neglects the effect of other components in the glass [35] and was calculated by dividing the mass of oxygen atoms in one mole of glass, m_o using equation 2:

$$m_o = M_o \times \left(5x_{P_2O_5} + x_{MgO} + x_{CaO} + 2x_{Na_2O} + 2x_{TiO_2}\right) \text{.....(2)}$$

(where, M_o is the atomic weight of oxygen and x is the mole fraction of oxide) by the molar volume of the glass, V_m , which was calculated by dividing the mass of 1 mole of glass by experimental density of the glass, *ρ (as shown in equation 3).*

$$V_m = \frac{x_{P_2O_5}M_{P_2O_5} + x_{MgO}M_{MgO} + x_{CaO}M_{CaO} + x_{Na_2O}M_{Na_2O} + x_{TiO_2}M_{TiO_2}}{\rho} \text{.....(3)}$$

Thermal analysis

The thermal properties of the phosphate-based glasses (PBGs), specifically the glass transition (T_g) (measured at the midpoint), onset of crystallisation (T_x), crystallisation peak (T_c), melting

peak (T_m) temperatures and glass stability against crystallisation, were characterised using a simultaneous thermal analysis instrument (SDT, TA Instruments SDT Q600, USA). Approximately 30 mg of glass powder (particle size range between 45-100 µm were used which were obtained by crushing the glass using Ball mill and followed by sieving through stainless still sieves) was placed into a platinum pan and then heated from room temperature to 1100 ^oC at different heating rates (i.e. 10, 15 and 20 $^oC\ min^{-1}$) under 50 mL min^{-1} of nitrogen gas flow. An empty pan was also analysed in order to determine the baseline which was then subtracted from the thermal traces using TA Universal Analysis 2000 software. Triplicate was used for this measurements.

Activation energy of crystallisation

The activation energy for crystallisation (E_c) associated with the crystallisation peak of the glasses was calculated using the Kissinger equation 4 [30].

$$\ln\left(\frac{\beta}{{T_c}^2}\right) = -\frac{E_c}{RT_c} + \text{Constant} \quad \text{.....(4)}$$

Where β is the heating rate, T_c is the crystallisation peak temperature measured at the different heating rates (i.e. 10, 15 and 20 $^oC\ min^{-1}$) and R is the gas constant.

The Johnson-Mehl-Avrami (JMA) exponent (n), provides information on the crystal growth dimensionality [29], and can be obtained using the equation proposed by Augis and Bennett [31] (see equation 5)

$$n = \frac{2.5\ {T_c}^2}{\Delta T_{FWHM}\frac{E_c}{R}} \quad \text{.....(5)}$$

Where n is the JMA exponent, T_c is the crystallisation peak temperature, ΔT_{FWHM} is the full width at half maximum of the crystallisation peak, E_c is the activation energy of crystallisation and R is the gas constant.

Fourier transform infrared (FTIR) spectroscopic analysis

Infrared spectroscopy was performed using a Bruker Tensor-27 spectrometer (Germany). All spectra were analysed using Opus^{TM} software version 5.5. The glass powders (particle size range 45-100 µm) were scanned in absorbance mode in the region of 4000 to 550 cm^{-1} (wave numbers) and the spectra were collected with a resolution of 4 cm^{-1} by averaging 32 scans using a standard pike attenuated total reflectance (ATR) cell (Pike technology, UK).

Micro Raman spectroscopic analysis

Micro Raman spectroscopy was performed using a Horiba JobinYvonLabRAM HR Raman spectrometer equipped with an automated *xyz* stage (Märzhäuser). Spectra were acquired over the range 100-1400 cm^{-1} using a 532 nm laser at 34 mW power, a 100x objective and a 50 µm confocal pinhole. To simultaneously scan a range of Raman shifts, a 600 lines mm^{-1} rotatable diffraction grating along a path length of 800 mm was employed. Spectra were detected using a Synapse CCD detector (1024 pixels) thermoelectrically cooled to −60 °C. Before spectra collection, the instrument was calibrated using the zero-order line and a standard Si (100) reference band at 520.7 cm^{-1}. The spectral resolution in this configuration is better than 1.8 cm^{-1}.

For single point measurements of all glass formulations, spectra were acquired with an acquisition time of 30 seconds and 8 accumulations to improve the signal to noise ratio, from five random locations and averaged to give a mean spectrum. For M8T1 (as a representative of a 1 mol% TiO_2 containing glass), a lateral map of the top surface of the glass was obtained by acquiring spectra at 2 µm steps within a square 40 x 40 µm (a total of 441 spectra). In this configuration, the spatial resolution was ~1 and ~3 µm in the lateral (xy) and axial (z) dimensions, respectively. As each individual spectrum was collected for 10 seconds, repeated

once in order to automatically remove the spikes due to cosmic rays, the whole map required approximately 2.5 hours of acquisition time. The intensity (as height) of the band in the region 845-940 cm^{-1} (a diagnostic vibrational mode the TiO_5 unit) was evaluated within the map using univariate analysis within Labspec 6 software. Optical micrographs of the glasses were obtained using a 100x objective lens.

Nuclear magnetic resonance (NMR) spectroscopic analysis

^{31}P NMR is used to evaluate the structural connectivity of the phosphate glass network [38].

^{31}P MAS NMR spectra were recorded at room temperature on a Varian Chemagnetics Infinityplus spectrometer operating at a Larmor frequency of 121.468 MHz using a 4 mm MAS probe spinning at 12.5 kHz. The ^{31}P $\pi/2$ pulse duration was 3.0 μs, the spectral width was 100 kHz and the acquisition time was 10.24 ms. Chemical shifts are quoted relative to 85% H_3PO_4 using $Na_4P_2O_7.10H_2O$ as an external secondary reference. Prior to acquiring quantitative ^{31}P spectra the spin-lattice relaxation time T_1 was determined for each sample by saturation recovery. Saturation was achieved by 100 ^{31}P $\pi/2$ pulses spaced by delays of between 5 and 20 ms with recovery delays of up to 1000 s. Quantitative ^{31}P NMR spectra required relaxation delays (5 T_1) of the order of between 60 s and 250 s depending on the sample. The resulting spectra were deconvoluted into a set of Gaussian lineshapes which were integrated in order to quantify the proportions of the different Q environments in the sample. First-order MAS sidebands were included in the analysis. Higher-order sidebands contained less than 1 % of the spectral intensity and were neglected.

Results

X-ray diffraction analysis

XRD traces of the glasses are presented in Figure 1. With the exception of M4T0 and M2T0 formulations, a single broad peak between 20° and 40° (2θ) was observed for all of the glass compositions. The absence of any sharp crystalline peak confirmed the amorphous nature of these glasses. The amorphous glasses were chosen for further characterisation in this study. As M2T0 and M4T0 crystallised during manufacture they were not studied further.

Density

Figure 2 shows the density of the glasses. As can be seen, the density decreased from 2745 to 2725 kgm^{-3} with decreasing MgO content from 24 to 8 mol% for the glasses that did not contain TiO_2. However, the titanium contianing glasses showed a higher density in comparison to M8T0.

Oxygen density and molar volume

Figures 3a and 3b present the oxygen density and molar volume of glasses with no TiO_2 and with 1 mol% TiO_2, respectively. As seen from Figure 3a, the oxygen density decreased from 1.30 to 1.25 gcm^{-3}, whereas the molar volume increased from 32.05 to 33.21 cm^3mol^{-1}, as the CaO content increased from 16 to 32 mol% (i.e. the MgO content correspondingly decreased from 24 to 8 mol%). For the glasses with 1 mol% TiO_2 (see Figure 3b), the oxygen density was seen to decrease from 1.26 to 1.24 gcm^{-3}, whereas molar volume was seen to increase from

33.1 to 33.5 cm^3mol^{-1}, with increasing CaO content from 32 to 38 mol% (or decreasing MgO content from 8 to 2 mol%).

Thermal properties

From Table 2, it has been observed that the glass transition (T_g), onset of crystallisation (T_x), crystallisation peak (T_c), initial melting (T_m) temperatures and the stability (ΔT) of the glasses against crystallisation were found to decrease with decreasing MgO content. It is to be noted that, the T_g, T_x, T_c and T_m values of some of these formulations (except for the M8T1 glass) have been reported previously [39]. However, in this investigation those values were utilised to calculate the glass stability in order to address their crystallisation behaviour, as presented in Table 2. The T_g value was seen to decrease from 448 °C (for M24T0) to 430 °C (for M8T0) with decreasing MgO content from 24 to 8 mol%. However, with the addition of 1 mol% of TiO_2, the M8T1 glass showed a 12 °C higher T_g value than M8T0. For the fixed 1 mol% TiO_2 content glasses, the T_g value was seen to decrease from 442 °C (for M8T1) to 436 °C (for M2T1) with decreasing MgO content from 8 to 2 mol%. Similarly, the T_c was seen to decrease from 571 °C (for M24T0) to 541 °C (for M2T1).

Crystallisation behaviour

As stated earlier, PBGs in the glass system $40P_2O_5$-(24-x)MgO-(16+x)CaO-(20-y)Na_2O-yTiO_2 (where $0 \leq x \leq 22$ and y=0 or 1) with MgO content 8 mol% and above 8 mol% were formed successfully, as confirmed by XRD analysis. However, further replacement of MgO with CaO showed a strong tendency towards crystallisation (i.e. M4T0 and M2T0 glasses, see Figure 1). On the other hand, the addition of 1 mol% TiO_2 in place of Na_2O for glasses with less than 8 mol% MgO (i.e. M4T1, M2T1) reduced the tendency of the glass to crystallise. Figure 4a and 4b show 2 mol% MgO containing glasses without and with 1 mol% TiO_2 content, respectively.

As the crystallisation temperature varied with glass particle sizes (see ESI Figure 1 for M24T0 as an example), a fixed particle size range of 45-100 μm was used to calculate the activation enery of cystallisation for all glass formulations. Figure 5 shows results for the M24T0 glass as an example of the effect of different heating rates on the crystallisation temperature. This process was repeated three times for each glass formulation. As can be seen, the crystallisation peak shifted to higher temperature (from 571 to 587^{o}C) and the peak intensity increased with increasing heating rate (from 10 to 20 ^{o}Cmin^{-1}). In order to calculate the activation energy of crystallisation, ln (β/T_c^2) over $1/T_c$ was plotted for all glass formulations (see ESI Figure 2 for M24T0 as an example) and the slope of these lines corresponds to $-E_c/R$ (where, R is the gas constant).

Table 3 provides values of the crystallisation peak temperatures obtained at the different heating rates, the activation energy of crystallisation (E_c) and the JMA exponent for the glasses. It was found that E_c decreased from 248 to 229 kJmol^{-1} as the content of MgO decreased from 24 to 8 mol% for glasses with no TiO_2. However, the M8T1 glass revealed an E_c value 38 kJmol^{-1} higher in comparison to M8T0. For the glasses containing 1 mol% TiO_2, the E_c was seen to decrease from 267 to 233 kJmol^{-1} with decreasing MgO content from 8 to 2 mol%.

FTIR and Raman spectroscopy

Figures 6a and 6b show the FTIR and Raman spectra collected from the fingerprint region for the glasses investigated. At least five (725, 900, 1000, 1100 and 1250 cm^{-1}) and eight (347, 500, 546, 700, 900, 1040, 1160 and 1260 cm^{-1}) vibrational modes associated with the

phosphate network [40-42] were observed in the FTIR and Raman spectra, respectively, the position and proposed assignments of which are presented in ESI Table 1.

Of note in the IR spectra (Figure 6a), the intensity of the peaks at ca. 900 and 1100 cm^{-1}, associated with asymmetric P-O-P stretching vibrations of bridging oxygens in Q^2 and Q^1 tetrahedra, respectively [9,42], were seen to increase with decreasing MgO content (from 24 to 8 mol%) for glasses containing no TiO_2. However, the M8T1 glass showed a lower peak intensity at the same positions relative to M8T0. Moreover, redshifting of bands from 739 to 729 cm^{-1} (ν_s(P-O-P), Q^2), from 899 to 889 cm^{-1} (ν_{as}(P-O-P), Q^2) and from 1119 to 1101 cm^{-1} (ν_{as}(P-O-P), Q^1) was observed with decreasing MgO content for the glasses containing no TiO_2. Interestingly, these same vibrational modes were blueshifted to a higher frequency for M8T1 relative to M8T0.

In the Raman spectra (Figure 6b), analogous redshifting of bands, such as those associated with the PO_2 symmetric stretching of non-bridging oxygen in Q^1 (from 1046 to 1042 cm^{-1}) and Q^2 (from 1161 to 1158 cm^{-1}) units, respectively,[43] was noted with decreasing MgO content. The position of these bands did not change for the Ti containing glasses. Likewise, the characterstic band at ca. 500 cm^{-1}, assigned to the bending vibrations of P-O bonds [43], redshifted from 503 to 497 cm^{-1} (for M24T0 and M8T0, respectively), remaining at 493 cm^{-1} for the Ti containing glasses. Furthermore, a distinctive band at 899 cm^{-1} was observed in the Raman spectra of the Ti containing glasses, assigned to the TiO_5 (titanyl) unit and a symmetric P-O stretch of phosphate interacting with Ti [44]. No evidence of a vibrational mode at ca. 640 cm^{-1}, diagnostic of the Ti-O stretch in TiO_6 octahedra, was noted. To explore the relative distribution of the TiO_5 component (899 cm^{-1}) within the glass, the top surface of M8T1 (as representative of the Ti containg glasses) was chemically mapped using Raman spectroscopy (Figure 7a). The resultant false colour image indicated that the 1 mol% TiO_2 was uniformly

distributed throughout the surface of the glasses, with the mean spectrum (Figure 7b) extracted from the map (441 spectra) matching well with that previously obtained from random, single point measurements.

NMR spectroscopy

Figure 8 shows ^{31}P MAS NMR spectra of the glasses. Two peaks were observed within the range of - 22.4 to -21.5 and -8.3 to -7.1 ppm. These ranges were assigned to Q^2 and Q^1 species, respectively [45]. The spectra showed that the peaks associated with Q^2 species shifted slightly from -22.44 to -21.75 ppm with substitution of MgO by CaO (from M24T0 to M8T0). ESI Table 2 provides peak positions and relative proportions of Q^1 and Q^2 species for the individual glasses. The proportion of Q^2 species for the glasses without Ti was found to be between 50 to 51%. No significant variation in the relative proportions was observed between the M8T0 and M8T1 glasses.

Discussion

Several researchers have investigated the crystallisation behaviour of different types of glasses [35,46-48] and report that crystallisation is strongly affected by the glass composition, heating rate and particle size [35,46]. In this current study, the effect of decreasing MgO (and hence increasing CaO) content and the addition of TiO_2 on glass formation ability was investigated for glasses in the system $40P_2O_5$-(24-x)MgO-(16+x)CaO-(20-y)Na_2O-yTiO_2 (where $0 \leq x \leq 22$ and y=0 or 1), including assessment of the physical, thermal, structural and crystallisation properties.

Density measurements give an indication of the degree of change in the glass structure with the variation of glass composition. The decrease in glass density from 2745 kgm^{-3} (for M24T0)

to 2725 kgm^{-3} (for M8T0) (see Figure 2) with reducing MgO content was attributed to the replacement of the higher density element Mg (1.74 gcm^{-3}) with the lower density element Ca (1.55 gcm^{-3}). Furthermore, the M8T1 glass showed a higher density than M8T0 which was attributed to the lower density element Na (0.97 gcm^{-3}) being replaced by the higher density element Ti (4.5 gcm^{-3}). A similar study conducted by Abou Neel *et al.* found that the density increased from 2.58 to 2.68 gcm^{-3} with the addition of 15 mol% TiO_2 into a ternary phosphate glass formulation [8]. They reported that the increase in density was due to the replacement of low density Na with higher density element Ti [8].

As seen from Figure 3, the oxygen density decreased, whilst the molar volume increased, with the substitution of MgO by CaO in this glass series. This was attributed to the fact that calcium has a larger ionic radius than magnesium, and as a result has lower polarising power due to its small charge to size ratio and subsequently lower attractive force to non-bridging oxygens (NBO) [35]. A similar finding was suggested by Al-noaman *et al.* who reported that the oxygen density increased from around 1.19 to 1.23 gcm^{-3} with the addition of 20 mol% MgO in place of CaO [35]. The compactness of the glasses in this study decreased with decreasing MgO content for the formulations containing no TiO_2. However, with the addition of 1 mol% TiO_2 the compactness of the structure increased as evidenced when compared to the oxygen density of the glass without TiO_2 (i.e. M8T0).

The thermal properties of phosphate-based glasses (PBGs) are strongly dependent on their structural features, such as chain length, cross-linking density and bonding strength. The decrease in T_g, T_x, T_c and initial melting temperature with decreasing MgO content for glasses that did not contain TiO_2 (see Table 2) was also attributed to the same reasons as discussed above for the oxygen density, i.e. due to the replacement of Mg-O bonds with Ca-O bonds.

The chemical bond strength of Mg-O is known to be higher than Ca-O, as Mg^{2+} has a smaller ionic radius (0.65 Å) compared to Ca^{2+} (0.99 Å) [49]. Furthermore, the smaller size of Mg results in a high charge to size ratio and thus exhibits higher electronegativity, which creates higher attractive forces to non-bridging oxygens (NBO) as compared to Ca [35]. Therefore, it was anticipated that Mg formed a strong cross-linking with phosphate chains, compare to Ca [50], which also correlated with a high compact structure for higher Mg content glasses as indicated by the oxygen density data.

The addition of 1 mol% TiO_2 was found to have increased T_g of M8T1, M4T1 and M2T1 in comparison to glass code M8T0. This increase in T_g was attributed to the replacement of Na-O bonds with Ti-O as Ti^{4+} ions have a higher field strength and greater bond strength than Na^+ [8,15]. A similar effect on T_g values for replacing Na^+ with Ti^{4+} was also observed in the $50P_2O_5$-30CaO-(20-x)Na_2O-xTiO_2 glass system investigated by Abou Neel *et al.* where the T_g values increased from 383 to 538 °C with addition of 15 mol% TiO_2 [8]. They suggested that the increase in T_g with addition of TiO_2 was due to the smaller ionic radius of Ti^{4+} (0.56 Å) compared to Na^+ (0.97 Å), where the size of ions (i.e. ionic radius) introduced into the glass network is a key factor in controlling their chemical durability and thermal stability. As TiO_2 has a smaller ionic radius and higher electrical charge than Na^+ it most likely generated stronger cross-linking between the phosphate chains via creating Ti–O–P links [51-53]. This finding also correlated with the compactness of the glass structure as the oxygen density increased with the addition of TiO_2.

The glass formation tendency of the formulations was seen to decrease with the substitution of MgO with CaO as the glass stability against crystallisation decreased from 106 °C (for M24T0) to 90 °C (for M8T0) (see Table 2). Formulations containing less than 8 mol% MgO in

the series investigated showed a strong tendency towards crystallisation (see Figure 4a). This was suggested to be due to the lower field strength of Ca^{2+}(0.33) as compared to Mg^{2+} (0.45) [54]. According to Dietzel, MgO can behave as an intermediate oxide [55] and in its intermediate state, can potentially act as a network former as well as a cross-linker between the phosphate chains [50,56,57]. On the other hand, Ca acts only as a network modifier and depolymerises the phosphate chains, which consequently increases the mobility of the phosphate structural groups in the melt [34]. As a result, the components can arrange themselves into an ordered crystalline structure more easily [34]. Therefore, for this glass series, a decrease in MgO content lead to an increase in crystallisation tendency. It has also been reported that the addition of TiO_2 to PBGs increased the glass stability by the formation of cross-links between the phosphate chains [21,52,53,58]. A number of studies have also suggested that titanium can enter the phosphate glass network as Ti^{4+} ions and thus behave as a glass network former [21,22]. Therefore, the crystallisation tendency may have been inhibited by the addition of 1 mol% TiO_2 (see Figure 4b).

Crystallisation is generally described by the activation energy for crystallisation (E_c) and the Johnson-Mehl-Avrami (JMA) exponent [47]. As seen from Figure 5, the crystallisation temperature and peak height increased with increasing heating rate. This could be attributed to the fact that the heat flow to the samples increased with increasing heating rate [35]. A similar result of increasing crystallisation peak intensity was also observed by Al-noaman *et al.* for silicate glasses, which increased from around 1 to 45 mcal/sec with increasing heating rate from 5 to 20 $^{o}Cmin^{-1}$ [35]. This result was also in good agreement with the results found by Clupper and Hench [59] and Bretcanu *et al.* [60]. Massera *et al*. also studied the effect of heating rate on the crystallisation peak intensity for $50P_2O_5$-40CaO-SrO-$10Na_2O$ glasses with particle sizes in the range 300-500 µm [47]. They reported that the crystallisation peak intensity

increased from 1.1 to 1.4 Wg^{-1} with increasing heating rate from 5 to 20 $^{o}Cmin^{-1}$ [47]. The changes in the width (broad vs narrow) of the crystallisation peaks are usually indicative of changes in the crystallisation mechanism [46]. The intensity of crystallisation peaks are often used to determine whether crystallisation has occurred at the surface or within the bulk of the materials [33,61]. A broad crystallisation peak can be associated with surface crystallisation whereas a sharp peak is associated with bulk crystallisation [46].

The decrease in E_c with decreasing MgO content for glasses containing no Ti content and the higher E_c for M8T1 (compared to M8T0) was attributed to the effect of field strength has been discussed above for oxygen density and thermal analysis. This result also correlated well with the glass stability (ΔT) data (shown in Table 2). Brauer *et al.* investigated the effect of TiO_2 on crystallisation behaviour in the P_2O_5-CaO-MgO-Na_2O glass system and reported that the activation energy increased from 270 to 360 $kJmol^{-1}$ with increasing TiO_2 content from 0 to 5 mol% due to the formation of higher cross-links between phosphate units [15]. The variation of E_c as a function of glass composition was in good agreement with the change in the crystallisation behaviour found by SDT analysis. Types of crystal growth must be determined for understanding the nucleation and growth kinetics of the first crystal that forms during heat treatment. During crystallisation of the glasses, the parameter, n, of the JMA model provides some insight into the crystal growth dimensionality [29]. The JMA exponent was calculated by the equation proposed by Augis and Benett [Eq 5] and shown in Table 3. Usually, n~1 is associated with surface crystallisation, n=2 with 2D and n=3 with 3D bulk crystallisation, with n>3 indicative of complex crystallisation behaviour[62].

FTIR and Raman spectra for the glasses showed small variations in terms of intensities and positions of peaks as a function of composition. These results were expected as the

substitution of MgO by CaO did not change the O/P ratio and hence no variation in Q species was expected. Similarly, no significant change in the relative proportion of Q^1 and Q^2 species was found from the ^{31}P NMR analysis and all of the glass formulations contained an almost equal percentage of Q^1 and Q^2. The small variations observed were within the error from the fitting. The redshift in the position of the symmetric and asymmetric P-O-P stretching modes observed in the FTIR spectra was consistent with the replacement of higher field strength Mg^{2+} by lower field strength Ca^{2+} and the replacement of lower field strength Na^+ ions by higher field strength Ti^{4+} ions [63], leading to increases in the P-O-P bond angle as a consequence of either longer phosphate chain lengths or the presence of larger cationic size [64]. A similar study was done by Abou Neel *et al.* who found that the asymmetric ν_{as}(P-O-P) stretching modes shifted to higher frequency and the peak intensity decreased with increasing SrO content due to the replacement of Na^+ ions by higher field strength of Sr^{2+} ions [9]. The increase in the intensity of the asymmetric ν_{as}(P-O-P) stretching modes with reducing MgO for the glasses containing no TiO_2 could be due to the decrease in phosphate-cation bonding interaction as Mg^{2+} has higher field strength than Ca^{2+} [9]. On the other hand, the Ti containing glasses showed broader peaks as compared to M8T0, which may have been due to Ti^{4+} increasing the phosphate-cation bonding interactions compared to Na^+ [9]. The bands at around 1000 and 1100 cm^{-1} were assigned to symmetric $\nu_s(PO_3)^{2-}$ and asymmetric $\nu_{as}(PO_3)^{2-}$ modes, respectively which are associated with Q^1 species [16,65]. The intensity of the absorption bands for asymmetric stretching modes, $\nu_{as}(PO_3)^{2-}$ of the chain terminating groups of the glasses increased with decreasing MgO content down to 8 mol%, which was an indication for decreasing the cross-links between the glass network and thereby reducing the rigidity of the network [41]. However, the addition of 1 mol% TiO_2 (i.e. M8T1) reduced the intensity (compared to M8T0) of the absorption bands for the asymmetric stretching modes, $\nu_{as}(PO_3)^{2-}$ significantly.

Similarly, this could be attributed to the increase in degree of polymerisation or creating more cross-linking between the glass network as Ti can act as a network former or network modifier [41].

From the mean Raman spectra, obtained by averaging point spectra collected from five random locations, a diagnostic peak for Ti containing glasses was observed at 899 cm^{-1}, associated with a Ti-O stretching vibration in TiO_5 (titanyl) units and confirming the role of TiO_2 as a network modifier [44]. Although subtle differences in the intensity of the red colouration were noted in the false colour spectroscopic map, associated with differences in surface topography, TiO_5 was found to be within every pixel of the map, indicating its uniform dispersion throughout the surface of the glass. No evidence for the presence of TiO_6 (titanate) units, which typically are observed at around 640 cm^{-1} in the Raman spectrum, and known to act as a network former [44], were found for the Ti containing glasses investigated.

The addition of 1 mol% TiO_2 to the phosphate glass network (in the glass series investigated) was shown to be sufficient to increase cross-linking between the phosphate chains, and was sufficient to reduce the crystallisation tendency of the lower Mg containing glasses in the glass system $40P_2O_5$-(24-x)MgO-(16+x)CaO-(20-y)Na_2O-yTiO_2 (where $0 \leq x \leq 22$ and y=0 or 1).

Conclusions

The glass forming ability for the composition with the replacement of MgO by CaO in 40P2O5-(24-x)MgO-(16+x)CaO-(20-y)Na2O-yTiO2 (where $0 \leq x \leq 22$ and y=0 or 1 glass system was investigated. The glass composition containing minimum 8 mol% MgO with no TiO2 formed fully amorphous glass. Further reducing the MgO (below 8 mol%) without TiO2 in the above

glass series showed strong tendency towards crystallisation. Interestingly, only 1 mol% TiO_2 inhibited the crystallisation for the lower MgO containing (M4T0, M2T0) glasses. The role of TiO_2 in the glass series investigated as a network modifier rather than network former.

Acknowledgements

The authors would like to thank the Nanoscale and Microscale Research Centre (NMRC) at the University of Nottingham for the help and support with Raman spectroscopy analyses. The author (M.T.I) would also like to acknowledge the financial support provided by the University of Nottingham, Faculty of Engineering (the Dean of Engineering Research Scholarship for International Excellence).

References

1. Rey C, Combes C, Drouet C, Glimcher MJ. Bone mineral: update on chemical composition and structure. Osteoporosis International 2009;20(6):1013-1021.
2. Rahaman MN, Day DE, Bal BS, Fu Q, Jung SB, Bonewald LF, Tomsia AP. Bioactive glass in tissue engineering. Acta biomaterialia 2011;7(6):2355-2373.
3. Ahmed I, Lewis M, Olsen I, Knowles J. Phosphate glasses for tissue engineering: Part 1. Processing and characterisation of a ternary-based P 2 O 5–CaO–Na 2 O glass system. Biomaterials 2004;25(3):491-499.
4. Neel EA, Ahmed I, Pratten J, Nazhat S, Knowles J. Characterisation of antibacterial copper releasing degradable phosphate glass fibres. Biomaterials 2005;26(15):2247-2254.

5. Abou Neel EA, O'Dell, Luke A., Smith, Mark E. and Knowles, Jonathan C. (2008) Processing, characterisation, and biocompatibility of zinc modified metaphosphate based glasses for biomedical applications. Journal of Materials Science: Materials in Medicine;19 (4):1669-1679.

6. Ahmed I, Neel EA, Valappil SP, Nazhat S, Pickup DM, Carta D, Carroll DL, Newport RJ, Smith ME, Knowles JC. The structure and properties of silver-doped phosphate-based glasses. Journal of Materials Science 2007;42(23):9827-9835.

7. Ahmed I, Collins C, Lewis M, Olsen I, Knowles J. Processing, characterisation and biocompatibility of iron-phosphate glass fibres for tissue engineering. Biomaterials 2004;25(16):3223-3232.

8. Neel EAA, Chrzanowski W, Knowles JC. Effect of increasing titanium dioxide content on bulk and surface properties of phosphate-based glasses. Acta biomaterialia 2008;4(3):523-534.

9. Neel EAA, Chrzanowski W, Pickup DM, O'Dell LA, Mordan NJ, Newport RJ, Smith ME, Knowles JC. Structure and properties of strontium-doped phosphate-based glasses. Journal of the Royal Society Interface 2008:rsif. 2008.0348.

10. Islam MT, Felfel RM, Abou Neel EA, Grant DM, Ahmed I, Hossain KMZ. Bioactive calcium phosphate–based glasses and ceramics and their biomedical applications: A review. Journal of tissue engineering 2017;8:2041731417719170.

11. Lankford K, Letourneau P. Evidence that calcium may control neurite outgrowth by regulating the stability of actin filaments. The Journal of cell biology 1989;109(3):1229-1243.

12. Ostomel TA, Shi Q, Tsung CK, Liang H, Stucky GD. Spherical bioactive glass with enhanced rates of hydroxyapatite deposition and hemostatic activity. Small 2006;2(11):1261-1265.

13. Kim CY, Clark AE, Hench LL. Early stages of calcium-phosphate layer formation in bioglasses. Journal of non-crystalline solids 1989;113(2-3):195-202.

14. Kokubo T, Kushitani H, Ohtsuki C, Sakka S, Yamamuro T. Effects of ions dissolved from bioactive glass-ceramic on surface apatite formation. Journal of Materials Science: Materials in Medicine 1993;4(1):1-4.

15. Brauer DS, Karpukhina N, Law RV, Hill RG. Effect of TiO 2 addition on structure, solubility and crystallisation of phosphate invert glasses for biomedical applications. Journal of Non-Crystalline Solids 2010;356(44):2626-2633.

16. Moustafa Y, El-Egili K. Infrared spectra of sodium phosphate glasses. Journal of non-crystalline solids 1998;240(1):144-153.

17. Martin S. Review of the structures of phosphate glasses. ChemInform 1991;22(17).

18. Brauer DS. Phosphate glasses. Bio-Glasses: An Introduction 2012:45-64.

19. Lee I-H, Shin S-H, Foroutan F, Lakhkar NJ, Gong M-S, Knowles JC. Effects of magnesium content on the physical, chemical and degradation properties in a MgO− CaO− Na 2 O− P 2 O 5 glass system. Journal of Non-Crystalline Solids 2013;363:57-63.

20. Shaim A, Et-Tabirou M. Role of titanium in sodium titanophosphate glasses and a model of structural units. Materials chemistry and physics 2003;80(1):63-67.

21. Kishioka A, Haba M, Amagasa M. Glass formation in multicomponent phosphate systems containing TiO 2. Bulletin of the Chemical Society of Japan 1974;47(10):2493-2496.

22. Nocuń M. Structural studies of phosphate glasses with high ionic conductivity. Journal of non-crystalline solids 2004;333(1):90-94.

23. Neel EA, Knowles J. Physical and biocompatibility studies of novel titanium dioxide doped phosphate-based glasses for bone tissue engineering applications. Journal of Materials Science: Materials in Medicine 2008;19(1):377-386.

24. Brauer DS, Rüssel C, Li W, Habelitz S. Effect of degradation rates of resorbable phosphate invert glasses on in vitro osteoblast proliferation. Journal of Biomedical Materials Research Part A 2006;77(2):213-219.

25. Navarro M, Ginebra MP, Planell JA. Cellular response to calcium phosphate glasses with controlled solubility. Journal of Biomedical Materials Research Part A 2003;67(3):1009-1015.

26. Dias A, Lopes M, Trigo Cabral A, Santos J, Fernandes M. In vitro studies of calcium phosphate glass ceramics with different solubility with the use of human bone marrow cells. Journal of Biomedical Materials Research Part A 2005;74(3):347-355.

27. Kasuga T, Hosoi Y, Nogami M, Niinomi M. Apatite formation on calcium phosphate invert glasses in simulated body fluid. Journal of the American Ceramic Society 2001;84(2):450-452.

28. Uhlmann DR. A kinetic treatment of glass formation. Journal of Non-Crystalline Solids 1972;7(4):337-348.

29. Joraid A. Limitation of the Johnson–Mehl–Avrami (JMA) formula for kinetic analysis of the crystallization of a chalcogenide glass. Thermochimica acta 2005;436(1):78-82.

30. Kissinger HE. Reaction kinetics in differential thermal analysis. Analytical chemistry 1957;29(11):1702-1706.

31. Augis J, Bennett J. Calculation of the Avrami parameters for heterogeneous solid state reactions using a modification of the Kissinger method. Journal of Thermal Analysis and Calorimetry 1978;13(2):283-292.

32. Marotta A, Buri A, Branda F. Surface and bulk crystallization in non-isothermal devitrification of glasses. Thermochimica Acta 1980;40(3):397-403.

33. Ray C, Day D. Identifying internal and surface crystallization by differential thermal analysis for the glass-to-crystal transformations. Thermochimica acta 1996;280:163-174.

34. Shelby JE. Introduction to glass science and technology: Royal Society of Chemistry; 2005.

35. Al-Noaman A, Rawlinson SC, Hill RG. The role of MgO on thermal properties, structure and bioactivity of bioactive glass coating for dental implants. Journal of Non-Crystalline Solids 2012;358(22):3019-3027.

36. Ray N. Composition—property relationships in inorganic oxide glasses. Journal of Non-Crystalline Solids 1974;15(3):423-434.

37. Fredholm YC, Karpukhina N, Law RV, Hill RG. Strontium containing bioactive glasses: glass structure and physical properties. Journal of Non-Crystalline Solids 2010;356(44):2546-2551.

38. Sharmin N, Hasan MS, Rudd CD, Boyd D, Werner-Zwanziger U, Ahmed I, Parsons AJ. Effect of boron oxide addition on the viscosity-temperature behaviour and structure of phosphate-based glasses. Journal of Biomedical Materials Research Part B: Applied Biomaterials 2016.

39. Islam MT, Hossain KMZ, Sharmin N, Parsons AJ, Ahmed I. Effect of magnesium content on bioactivity of near invert phosphate-based glasses. International Journal of Applied Glass Science 2017;8(4):391-402.

40. Kiani A, Hanna JV, King SP, Rees GJ, Smith ME, Roohpour N, Salih V, Knowles JC. Structural characterization and physical properties of P 2 O 5–CaO–Na 2 O–TiO 2 glasses by Fourier transform infrared, Raman and solid-state magic angle spinning nuclear magnetic resonance spectroscopies. Acta biomaterialia 2012;8(1):333-340.

41. Carta D, Pickup DM, Knowles JC, Ahmed I, Smith ME, Newport RJ. A structural study of sol–gel and melt-quenched phosphate-based glasses. Journal of non-crystalline solids 2007;353(18):1759-1765.

42. Valappil SP, Ready D, Neel EAA, Pickup DM, Chrzanowski W, O'Dell LA, Newport RJ, Smith ME, Wilson M, Knowles JC. Antimicrobial gallium-doped phosphate-based glasses. Advanced functional materials 2008;18(5):732-741.

43. Tiwari B, Dixit A, Kothiyal G, Pandey M, Deb S. Preparation and characterization of phosphate glasses containing titanium. Barc Newsletter 2007;285:167.

44. Brauer DS, Karpukhina N, Law RV, Hill RG. Effect of TiO2 addition on structure, solubility and crystallisation of phosphate invert glasses for biomedical applications. Journal of Non-Crystalline Solids 2010;356(44-49):2626-2633.

45. Brow RK. Review: the structure of simple phosphate glasses. Journal of Non-Crystalline Solids 2000;263:1-28.

46. Massera J, Fagerlund S, Hupa L, Hupa M. Crystallization mechanism of the bioactive glasses, 45S5 and S53P4. Journal of the American Ceramic Society 2012;95(2):607-613.

47. Massera J, Mayran M, Rocherullé J, Hupa L. Crystallization behavior of phosphate glasses and its impact on the glasses' bioactivity. Journal of Materials Science 2015;50(8):3091-3102.

48. Massera J, Hupa L, Hupa M. Influence of the partial substitution of CaO with MgO on the thermal properties and in vitro reactivity of the bioactive glass S53P4. Journal of Non-Crystalline Solids 2012;358(18):2701-2707.

49. Navarro JMF. El vidrio: Consejo Superior de Investigaciones Científicas; 1991.

50. Morikawa H, Lee S, Kasuga T, Brauer DS. Effects of magnesium for calcium substitution in P 2 O 5–CaO–TiO 2 glasses. Journal of Non-Crystalline Solids 2013;380:53-59.

51. Rajendran V, Devi AG, Azooz M, El-Batal F. Physicochemical studies of phosphate based P 2 O 5–Na 2 O–CaO–TiO 2 glasses for biomedical applications. Journal of non-crystalline solids 2007;353(1):77-84.

52. VOGEL J, Wange P, Knoche S, RÜSSEL C. Chemical solubility of phosphate glasses in the system Na2O-CaO-MgO-P2O5-Al2O3-TiO2 in aqueous solutions of different pH values. Glass science and technology 2004;77(2):82-87.

53. Wange P, VOGEL J, Knoche S, RÜSSEL C. Crystallization and viscosity of phosphate melts in the system Na2O-CaO-MgO-P2O5-Al2O3-TiO2. Glass science and technology 2004;77(4):172-176.

54. Kasuga T, Hattori T, Niinomi M. Phosphate glasses and glass-ceramics for biomedical applications. Phosphorus Research Bulletin 2012;26(0):8-15.

55. Dietzel A. Strukturchemie des Glases. Die Naturwissenschaften: Springer; 1941. p 537-547.

56. Karakassides M, Saranti A, Koutselas I. Preparation and structural study of binary phosphate glasses with high calcium and/or magnesium content. Journal of Non-Crystalline Solids 2004;347(1):69-79.

57. Parsons A, Ahmed I, Rudd C, Cuello G, Pellegrini E, Richard D, Johnson M. Neutron scattering and ab initio molecular dynamics study of cross-linking in biomedical phosphate glasses. Journal of Physics: Condensed Matter 2010;22(48):485403.

58. Vogel J, Wange P, Hartmann P. Effect of composition changes on the structure and properties of phosphate glasses in the pyrophosphate region. Glass science and technology 1997;70(1):23-27.

59. Clupper D, Hench L. Crystallization kinetics of tape cast bioactive glass 45S5. Journal of non-crystalline solids 2003;318(1):43-48.

60. Bretcanu O, Chatzistavrou X, Paraskevopoulos K, Conradt R, Thompson I, Boccaccini AR. Sintering and crystallisation of 45S5 Bioglass® powder. Journal of the European Ceramic Society 2009;29(16):3299-3306.

61. Li W, Mitchell BS. Nucleation and crystallization in calcium aluminate glasses. Journal of non-crystalline solids 1999;255(2):199-207.

62. Çelikbilek M, Ersundu AE, Aydın S. Crystallization kinetics of amorphous materials: INTECH Open Access Publisher; 2012.

63. Shih P-Y, Shiu H-M. Properties and structural investigations of UV-transmitting vitreous strontium zinc metaphosphate. Materials Chemistry and Physics 2007;106(2):222-226.

64. Shih P. Properties and FTIR spectra of lead phosphate glasses for nuclear waste immobilization. Materials chemistry and physics 2003;80(1):299-304.

65. Byun J-O, Kim B-H, Hong K-S, Jung H-J, Lee S-w, Izyneev A. Properties and structure of RO Na2O Al2O3 P2O5 (R= Mg, Ca, Sr, Ba) glasses. Journal of non-crystalline solids 1995;190(3):288-295.

List of Figures:

Figure 3: *Variaion of molar volume (M.V) and oxygen density (O.D) as a function of CaO content: a) with no TiO_2 and b) with 1 mol% TiO_2 present.*

Figure 4: *Images of 2 mol% MgO containing glass after casting to room temperature with a) no TiO_2 and b) 1 mol% TiO_2 content present.*

Figure 5 : *Variaion of the crystallisation peak as a function of different heating rates (10, 15 and 20 $^oCmin^{-1}$) for M24T0 glass (particle size 45-100 µm).*

Figure 6: *a) FTIR spectra and b) mean Raman spectra (N=5) for the glasses in the system of $40P_2O_5$-(24-x)MgO-(16+x)CaO-(20-y)Na_2O-yTiO_2 (*where 0≤x≤22 and y=0 or 1*). Spectra were averaged from those collected at five different, random locations on the top surface of the glass, with minimal spectral variation indicating a high degree of homogeneity.*

Figure 7: *a) (i) Optical image, (ii) Raman spectroscopic map overlaid on optical image and (ii) Raman spectroscopic map, including intensity scale bar and b) the mean Raman spectrum extracted from all spectra collected within the mapped area for M8T1 glass.*

Figure 8: *^{31}PNMR spectra for glasses in the system $40P_2O_5$-(24-x)MgO-(16+x)CaO-(20-y)Na_2O-yTiO_2 (*where 0≤x≤22 and y=0 or 1*).*

Electronic Supplimentary Information (ESI)

ESI Figure 1 : *Variaion of the crystallisation peak as a function of different particle sizes (45-100, 125-200 and 350-500 µm) at 20 $^oCmin^{-1}$ heating rate for M24T0 glass.*

ESI Figure 2: *The Plot of ln (β/T_C^2) vs $1/T_C$ for M24T0 glass (n=3).*

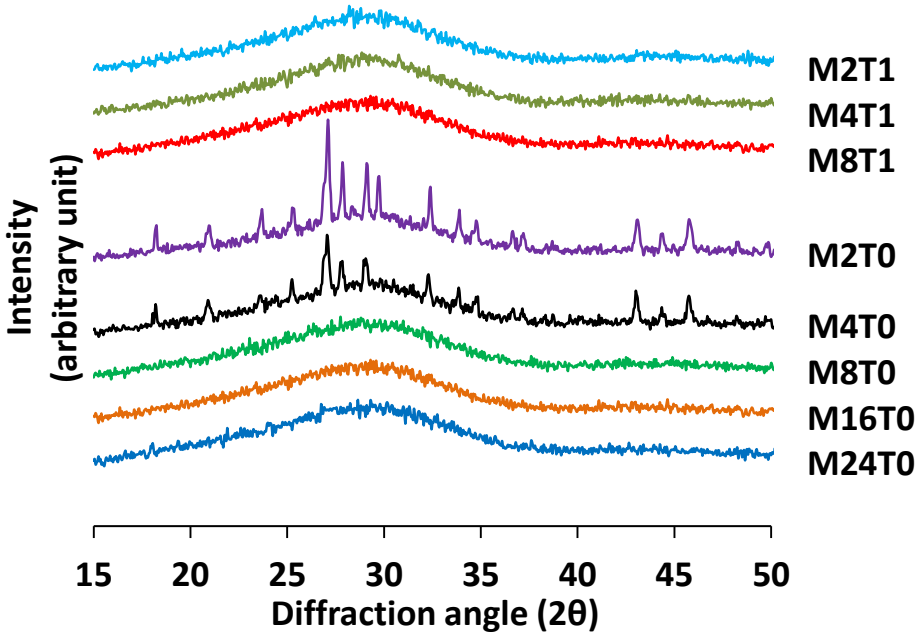

Figure 1: *X-ray diffraction patterns for glasses in the system 40P_2O_5-(24-x)MgO-(16+x)CaO-(20-y)Na_2O- yTiO_2 (*where 0≤x≤22 and y=0 or 1*). Crystalline phase for M4T0 and M2T0 was indexed with alpha-calcium pyrophosphate (α- $Ca_2P_2O_7$) (ICDD No. 00-009-0345).*

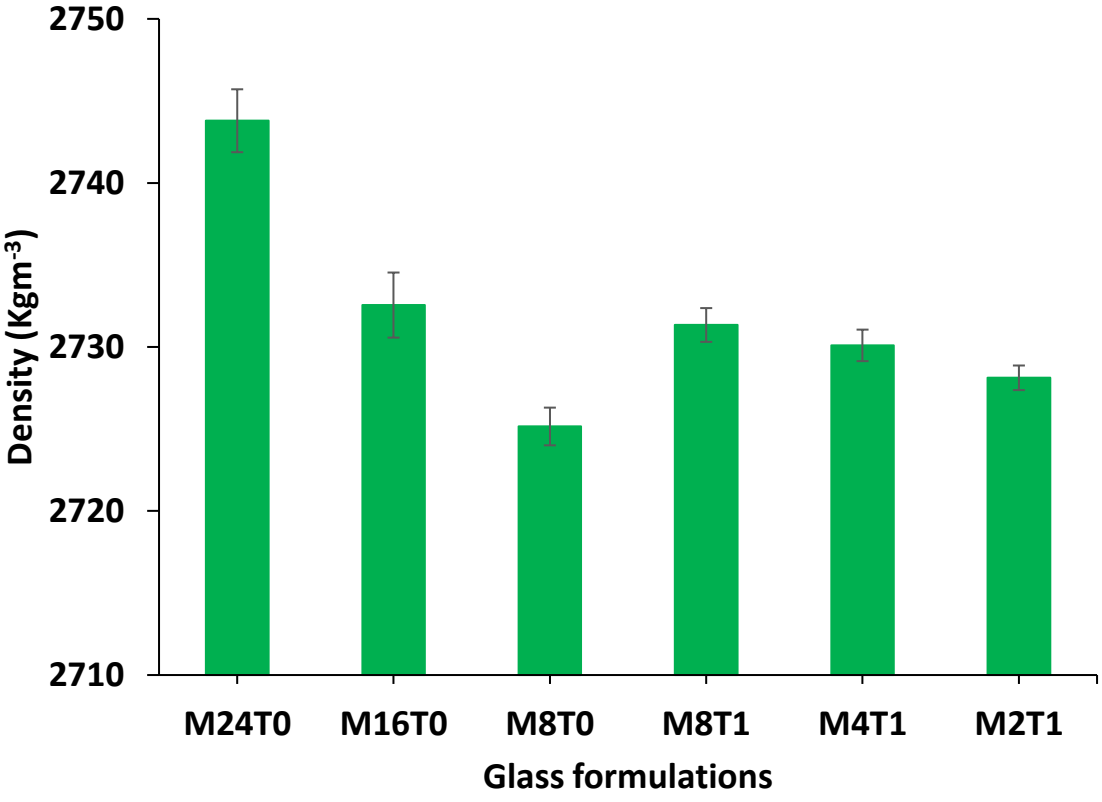

Figure 2: *Density of different glass formulations measured using the Archimedes method at room temperature.*

1 (a)

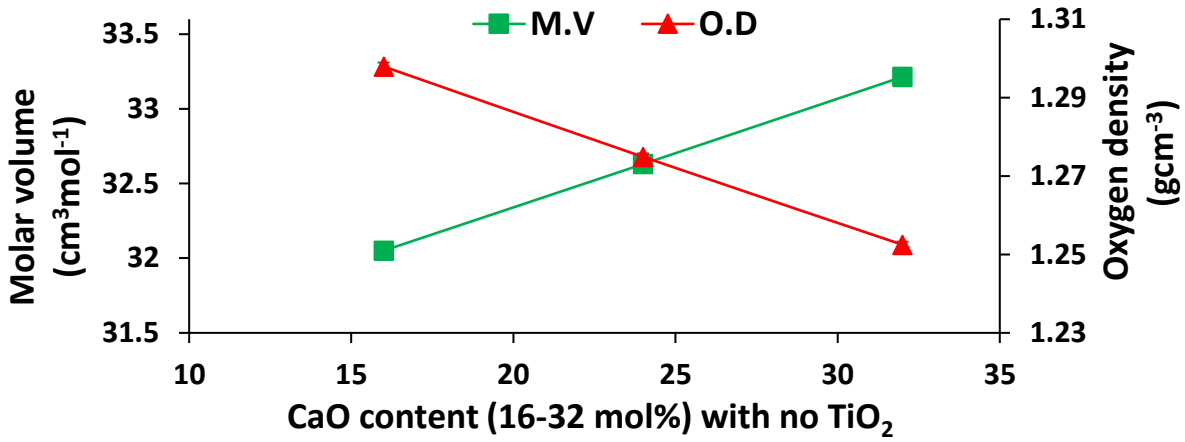

1.1 (b)

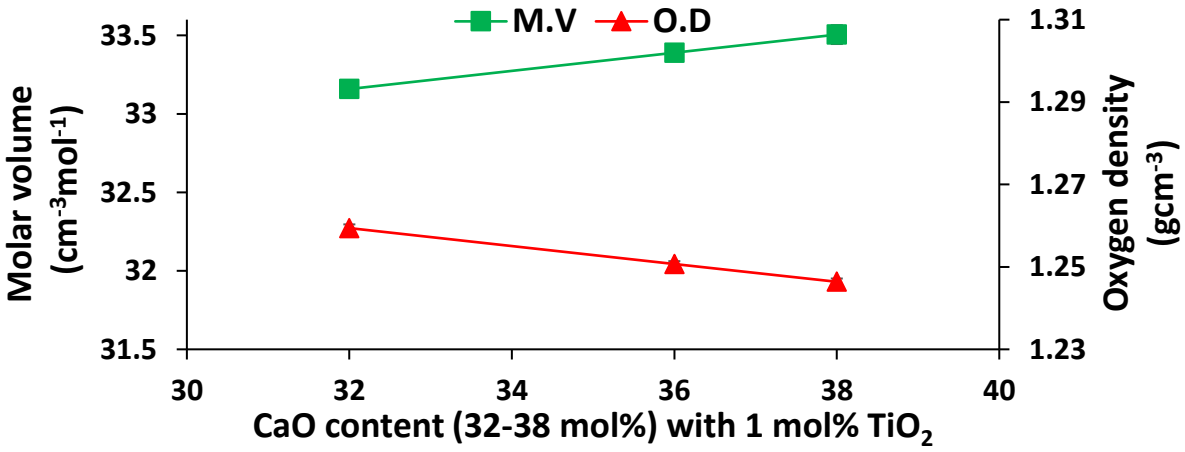

Figure 3: *Variation of molar volume (M.V) and oxygen density (O.D) as a function of CaO content: a) with no TiO_2 and b) with 1 mol% TiO_2 present.*

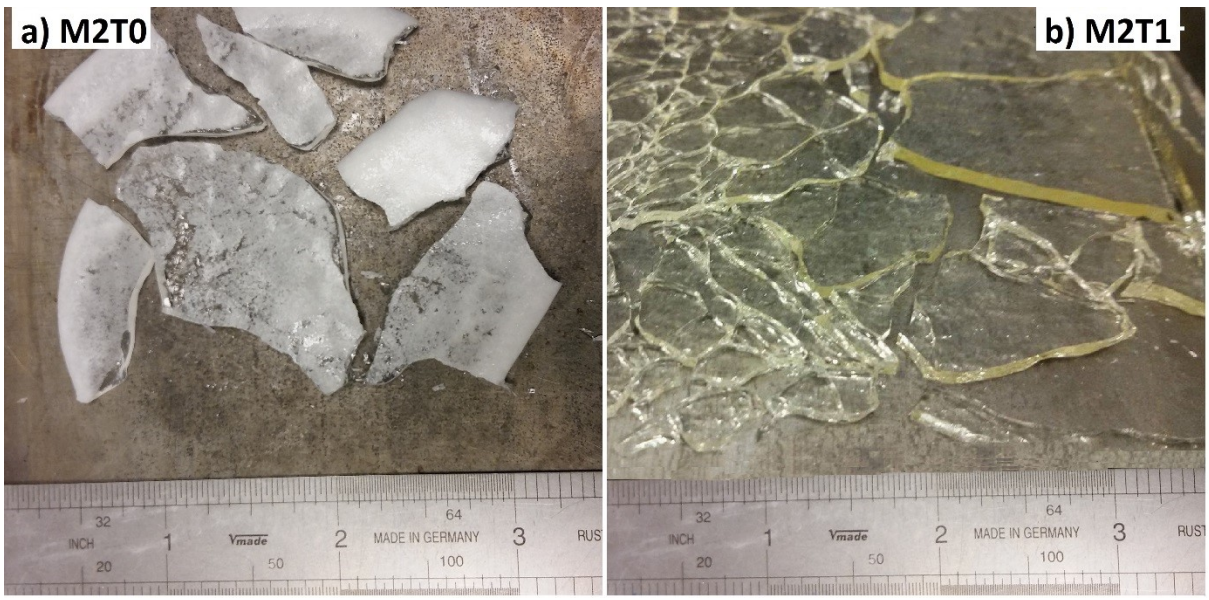

Figure 4: *Images of 2 mol% MgO containing glass after casting to room temperature with a) no TiO_2 and b) 1 mol% TiO_2 content present.*

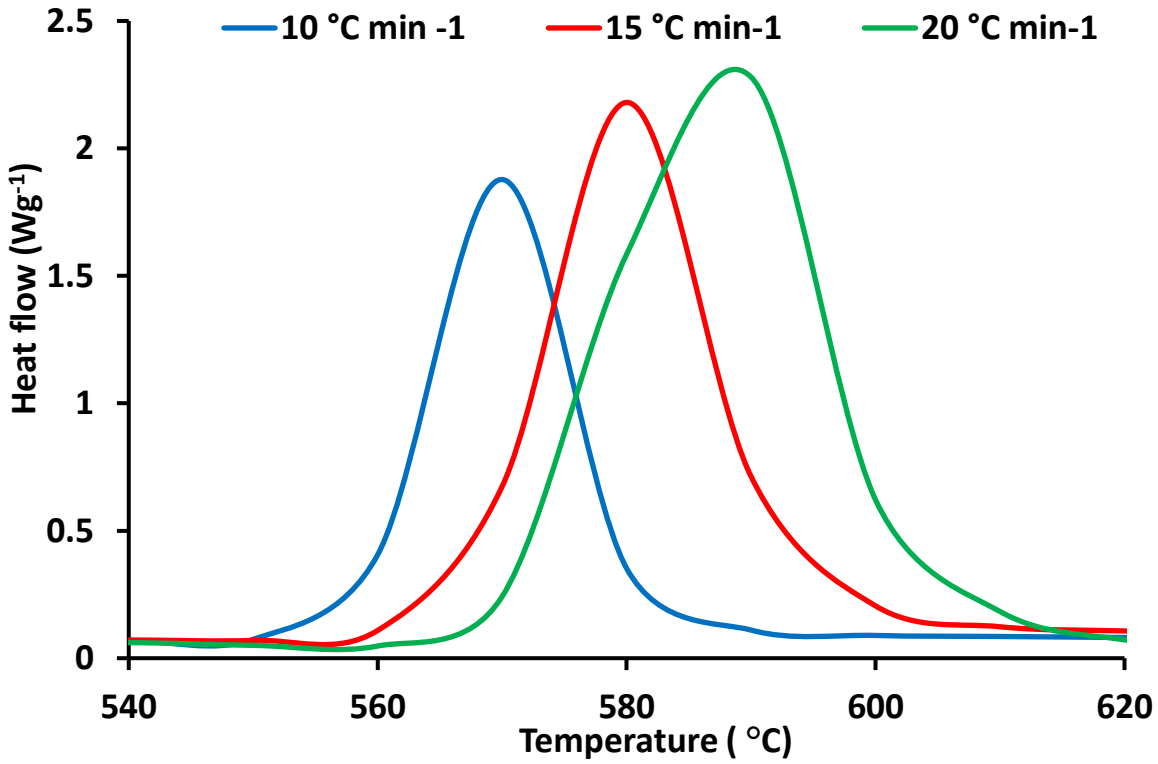

Figure 5 : *Variation of the crystallisation peak as a function of different heating rates (10, 15 and 20 $^{o}Cmin^{-1}$) for M24T0 glass (particle size 45-100 µm).*

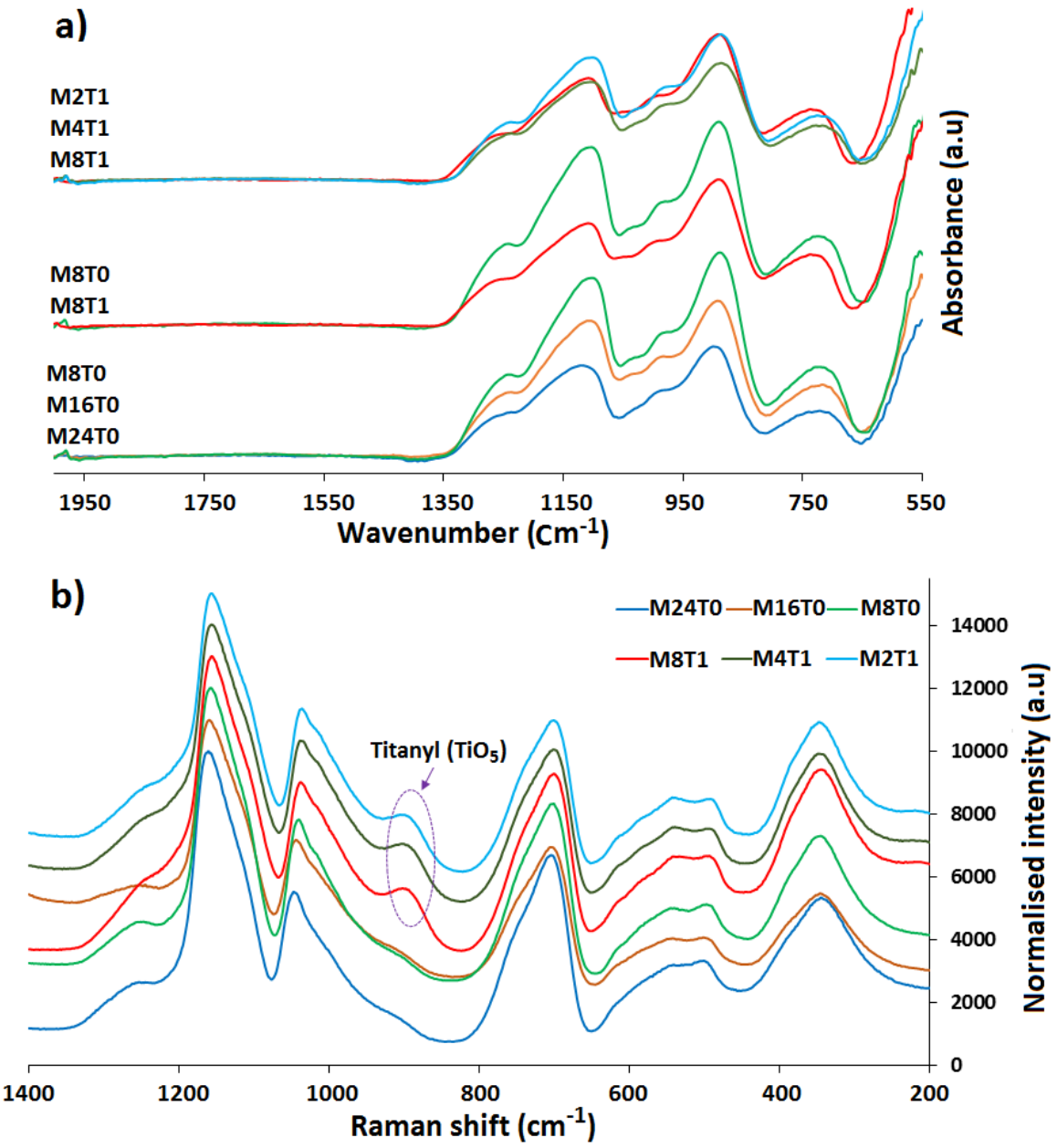

Figure 6: *a) FTIR spectra and b) mean Raman spectra (N=5) for the glasses in the system of* $40P_2O_5$-$(24-x)MgO$-$(16+x)CaO$-$(20-y)Na_2O$-$yTiO_2$ (where $0 \leq x \leq 22$ and $y=0$ or 1). *Spectra were averaged from those collected at five different, random locations on the top surface of the glass, with minimal spectral variation indicating a high degree of homogeneity.*

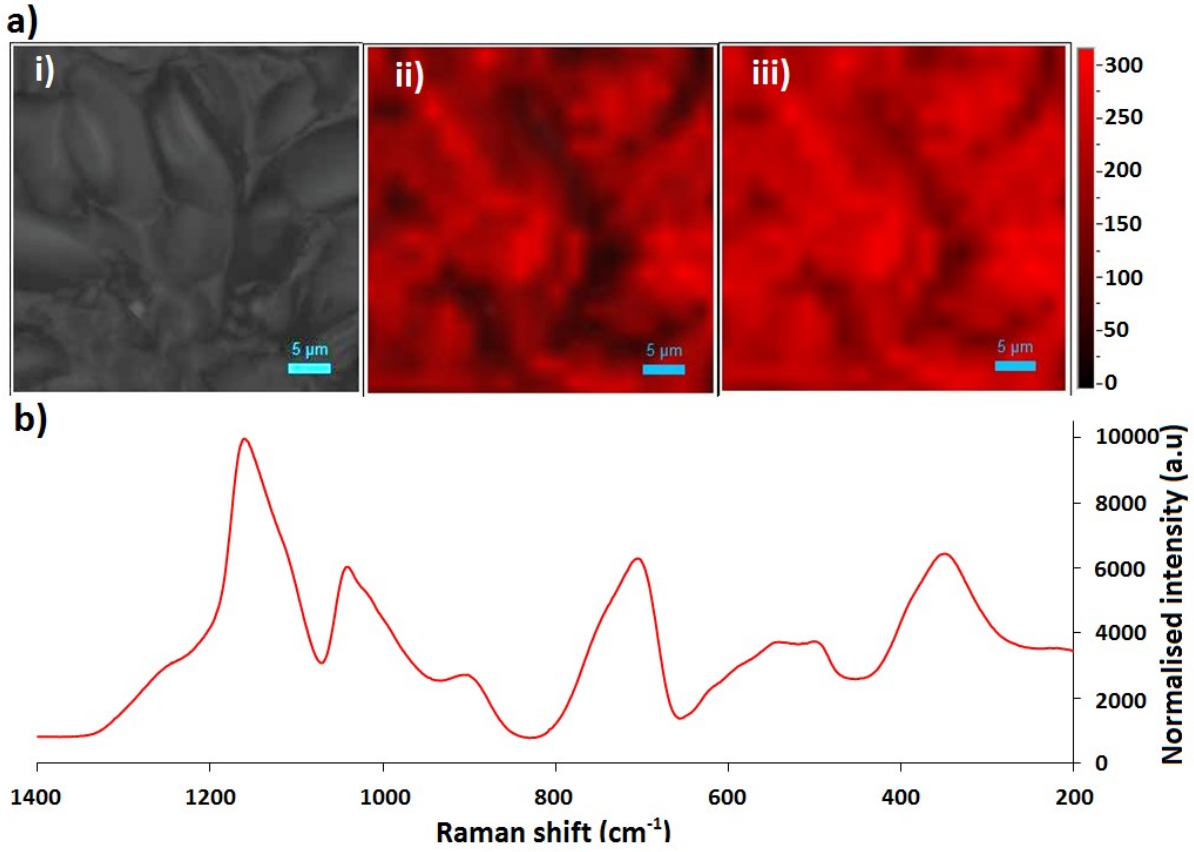

Figure 7: *a) (i) Optical image, (ii) Raman spectroscopic map overlaid on optical image and (ii) Raman spectroscopic map, including intensity scale bar and b) the mean Raman spectrum extracted from all spectra collected within the mapped area for M8T1 glass.*

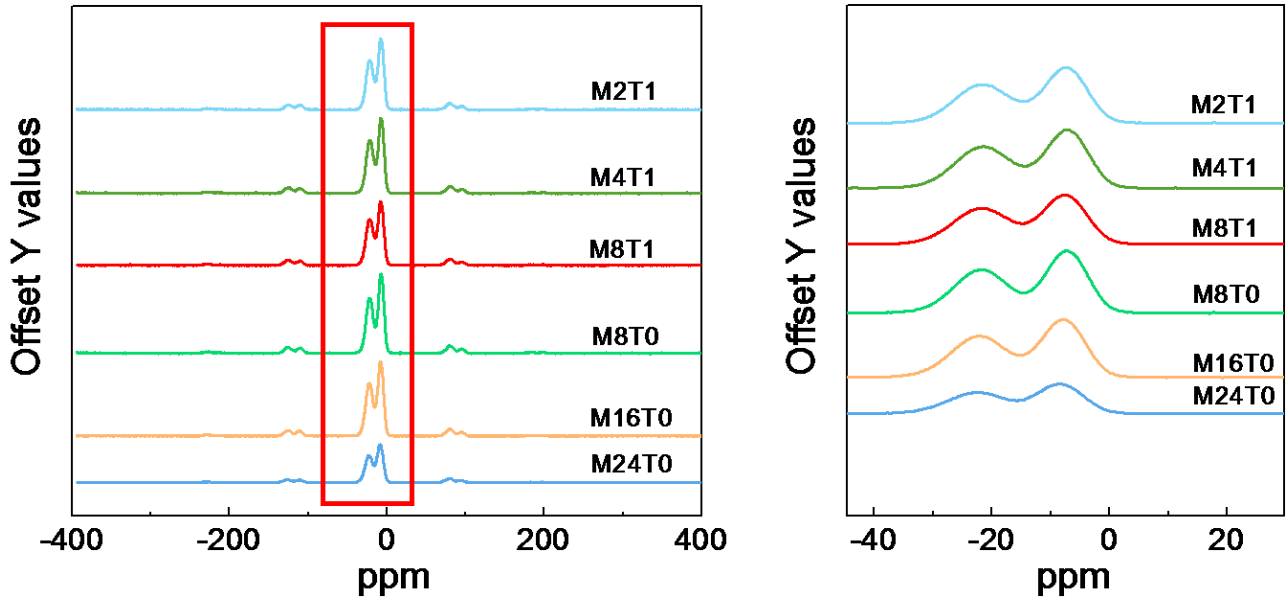

Figure 8: *^{31}PNMR spectra for glasses in the system $40P_2O_5$-(24-x)MgO-(16+x)CaO-(20-y)Na_2O-$yTiO_2$ (*where 0≤x≤22 and y=0 or 1*).*